Monthly Notices of the ROYAL ASTRONOMICAL SOCIETY

MNRAS **527,** 4076–4086 (2024) https://doi.org/10.1093/mnras/stad3467
Advance Access publication 2023 November 10

Single-lined eclipsing binaries with δ Scuti components: GQ Dra, RR Lep, and TYC 683-640-1

F. Kahraman Aliçavuş [1,2]★ F. Aliçavuş [1,2] Ç. G. Çoban [3] G. Handler[4] and P. De Cat [5]

[1]*Çanakkale Onsekiz Mart University, Faculty of Sciences, Physics Department, 17100, Çanakkale, Türkiye*
[2]*Çanakkale Onsekiz Mart University, Astrophysics Research Center and Ulupınar Observatory, TR-17100, Çanakkale, Türkiye*
[3]*Çanakkale Onsekiz Mart University, School of Graduate Studies, Department of Space Sciences and Technologies, TR-17100, Çanakkale, Türkiye*
[4]*Nicolaus Copernicus Astronomical Center, Polish Academy of Sciences, Bartycka 18, PL-00-716 Warsaw, Poland*
[5]*Royal Observatory of Belgium, Ringlaan 3, B-1180 Brussel, Belgium*

Accepted 2023 November 7. Received 2023 November 7; in original form 2023 September 26

ABSTRACT

Eclipsing binaries with (a) pulsating component(s) are remarkable objects to investigate the evolution and structure of stellar systems. Detailed studies of such systems are also important to reveal their pulsation properties. The largest sample of pulsating eclipsing binaries is the one containing δ Scuti variables. In this study, we present a comprehensive spectroscopic and photometric study of three such systems, GQ Dra, RR Lep, and TYC 683-640-1. Their orbital parameters were derived from their large-amplitude radial velocity variations. All systems were found to be single-lined eclipsing binaries. We determined the atmospheric parameters of the primary components, which are the more luminous ones. By using the results of the spectroscopic analysis, the binarity of the systems was modelled and the fundamental stellar parameters **(mass, radius)** of each system were obtained. In addition, the pulsations of the systems were analysed. Both GQ Dra and RR Lep exhibit frequencies that are modulated with the orbital period. Therefore, the pulsating components of these systems are identified as candidate tidally tilted pulsators.

Key words: stars: atmospheres – binaries: eclipsing – stars: fundamental parameters – stars: variables: δ Scuti.

1 INTRODUCTION

The importance of eclipsing binary systems has been known for over a century. These systems are one of the most popular objects in astrophysical studies because such systems play a key role in the understanding of stellar evolution and structure. Eclipsing binaries provide accurate stellar parameters (e.g. mass M, radius R) that are essential for theoretical modelling.

The discovery of pulsations in eclipsing binaries increases the popularity of these systems. Heretofore, a few different types of pulsating variables were found in eclipsing binaries (Lampens 2021). One of these types of pulsating stars is the δ Scuti variables. The δ Scuti stars are A-F spectral type systems that generally exhibit pulsations in pressure, gravity, and/or mixed modes with frequencies ranging from $\sim$5 to 72 d^{-1} (Aerts, Christensen-Dalsgaard & Kurtz 2010; Chang et al. 2013). Their interior can be probed by studying their pulsations with asteroseismic methods. δ Scuti stars are found in different evolutionary stages. Hence, the investigation of such systems is ideal for an in-depth examination of stellar evolution.

Many δ Scuti stars were discovered in eclipsing binary systems (Kahraman Aliçavuş et al. 2017; Liakos & Niarchos 2017). Their number is still increasing thanks to the observations provided by space telescopes (Kahraman Aliçavuş et al. 2022, 2023). It is known that δ Scuti variables in binaries show a different pulsational behavior because of the gravitational effects of the other binary component. The latest example of the gravitational effect on the pulsating components in binaries is the discovery of the tidally tilted pulsators. Handler et al. (2020) found the first one of these systems by showing that, due to tidal effects, the pulsation axis is changed and aligned with the orbital axis. After this discovery, a few additional members were found (e.g. CO Cam, Kurtz et al., 2020, TZ Dra, Kahraman Aliçavuş et al., 2022). However, the number of currently known tidally tilted pulsators is too low for a detailed understanding of the properties of this type of object.

A comprehensive investigation of δ Scuti pulsators in eclipsing binaries would be useful to comprehend δ Scuti variables and their pulsational structure. Therefore, in this study, we aim to analyse three eclipsing binaries with a δ Scuti component, GQ Dra, RR Lep, and TYC 683-640-1. GQ Dra was first classified as a variable by ESA (1997). It is listed as an eclipsing binary with a δ Scuti pulsator by Liakos & Niarchos (2017). Ulaş et al. (2020) presented the first detailed study of GQ Dra by analysing its orbital and pulsational variations. The variability of RR Lep has already been known for nearly a century (Hoffmeister 1931). It has been studied by several authors. Liakos & Niarchos (2013) examined the orbital and pulsational variations of this system. The binarity of RR Lep was also modelled by Erdem & Öztürk (2016), and, in addition, they gave the analysis of the orbital period variations. A detailed study for TYC 683-640-1 was given by Ulaş et al. (2022), and they presented the first binary modelling and pulsational analysis of this variable.

However, none of these systems were analysed with both photometric and spectroscopic data except for GQ Dra. For this study,

★ E-mail: filizkahraman01@gmail.com

© 2023 The Author(s)
Published by Oxford University Press on behalf of Royal Astronomical Society. This is an Open Access article distributed under the terms of the Creative Commons Attribution License (https://creativecommons.org/licenses/by/4.0/), which permits unrestricted reuse, distribution, and reproduction in any medium, provided the original work is properly cited.

Downloaded from https://academic.oup.com/mnras/article/527/2/4076/7408619 by Canakkale Onsekiz Mart Universitesi user on 03 January 2024

Table 1. Information related to the used photometric and spectroscopic observations. SNR represents the signal-to-noise ratio. Reference: [a] Stassun et al. (2019), [b] Høg et al. (2000), [c] Kreiner (2004), and [d] Ulaş et al. (2022).

Target name	V (mag)	Orbital period (d)	TESS Sector	Spectroscopic Obs. date	Number of spectra	Average SNR
GQ Dra	8.94 (3)[a]	0.76591(4)[c]	40, 47, 51, 53	May 2020–August 2020	33	62
RR Lep	10.14 (3)[b]	0.91543(4)[c]	5	October 2022–March 2023	20	50
TYC 683-640-1	9.71 (3)[b]	2.46170(6)[d]	5	November 2020–March 2023	22	60

Table 2. The results of the v_r analysis. The subscripts p and s represent the primary and secondary components, respectively. [a] shows the fixed parameters. The errors are given in parentheses in units of the last decimal. $f(m_p, m_s)$ is the mass function.

Parameter	GQ Dra	RR Lep	TYC 683-640-1
T_p (HJD)	2452500.07988 (11)	2452400.07710 (74)	2458001.01878 (79)
P_{orb}[a]	0.765905 (1)	0.915599 (1)	2.461820 (2)
γ (km s^{-1})	−15.1 (3)	−4.3 (3)	−15.9 (1)
K_p (km s^{-1})	83.4 (5)	61.4 (3)	76.8 (2)
e	0.000 (1)	0.000 (4)	0.000 (5)
ω (deg)	90.0 (5)	90.0 (6)	90.0 (6)
$a_p \sin i$ ($R_\odot$)	1.262 (8)	1.111 (6)	3.737 (10)
$f(m_p, m_s)$ ($M_\odot$)	0.0460 (8)	0.0220 (4)	0.1157 (9)

we collected high-resolution spectroscopic data and added them to the available space-based photometric data of the systems to analyse them comprehensively. The paper is organized as follows. Information about the observational data is given in Section 2. The spectroscopic analysis, including radial velocity measurements and the determination of the atmospheric parameters, is presented in Section 3. In Section 4, the photometric analyses (binary modelling and pulsational analysis) are introduced. We end in Section 5 with a discussion and an overview of conclusions.

2 OBSERVATIONAL DATA

The photometric data of GQ Dra, RR Lep, and TYC 683-640-1 were collected with the *TESS* (Ricker et al. 2014). *TESS* observes almost the entire sky by dividing it into sectors that are each observed for ∼27 d. *TESS* observations are carried out with short (120 s) and long (200, 600, and 1800 s) cadences. Since in this study we also aim to investigate the pulsational behavior of the targets, we used the available *TESS* short cadence data or 600 s long cadence mode as their Nyquist frequencies are high enough for the study of δ Scuti-type variations. The *TESS* photometry of the targets was taken from the Barbara A. Mikulski Archive for Telescopes (MAST).[1] Two types of TESS fluxes are provided: Simple Aperture Photometry (SAP) and Pre-search Data Conditioning SAP (PDCSAP). The SAP data are used in our study since there were no significant differences between the two fluxes. We converted them into magnitudes by using the equation given by Kahraman Aliçavuş et al. (2022). GQ Dra has 200 s (S57) and 600 s cadence data in four different sectors (S40, S47, S51, S53) while data observed in 120 s cadence mode is available in only one sector for RR Lep (S5) and TYC 683-640-1 (S5). Additionally, RR Lep (S5), and TYC 683-640-1 were observed with 600 s cadence mode in sector 32. In the study, we used 120 s data for RR Lep (S5), and TYC 683-640-1 because its Nyquist frequency reaches up to 350d^{-1}. For GQ Dra, 600 s data were taken into account as those were taken in four different sectors, and by combining those data we could reach a higher signal-to-noise level (SNR) . In Table 1, information about the used *TESS* data is given.

The spectroscopic data of the target stars were taken with the *High Efficiency and Resolution Mercator Échelle Spectrograph* (HERMES; Raskin et al. 2011) HERMES provides spectra with a resolving power of ∼85 000 and in the wavelength range 377–900 nm. For each target, we collected spectra that were spread over the orbital period to provide more accurate results in the spectroscopic analyses. The collected spectra were reduced with the dedicated pipeline taking into account the classical reduction steps such as bias subtraction, flat field correction, and wavelength calibration. The reduced spectra were then normalized manually utilizing the IRAF[2] *continuum* (Tody 1986) task. Information about the photometric and spectroscopic data is given in Table 1.

3 SPECTROSCOPIC ANALYSIS

Spectroscopic data of the systems were analysed to derive the radial velocities, obtain the orbital parameters, and determine the atmospheric parameters of the binary components. These analyses were carried out in advance of the photometric ones because some parameters determined from the spectroscopy are used as input to obtain precise results from photometry.

3.1 Radial velocity analysis

The radial velocity (v_r) measurements of the systems were done using the *FXCOR* task of IRAF. This task calculates the v_r values with the cross-correlation technique by using a spectrum of a standard star or a synthetic spectrum as a template in the calculation. Therefore, in this analysis, we generated some synthetic spectra considering the TESS

[1] https://mast.stsci.edu

[2] http://iraf.noao.edu/

Downloaded from https://academic.oup.com/mnras/article/527/2/4076/7408619 by Canakkale Onsekiz Mart Universitesi user on 03 January 2024

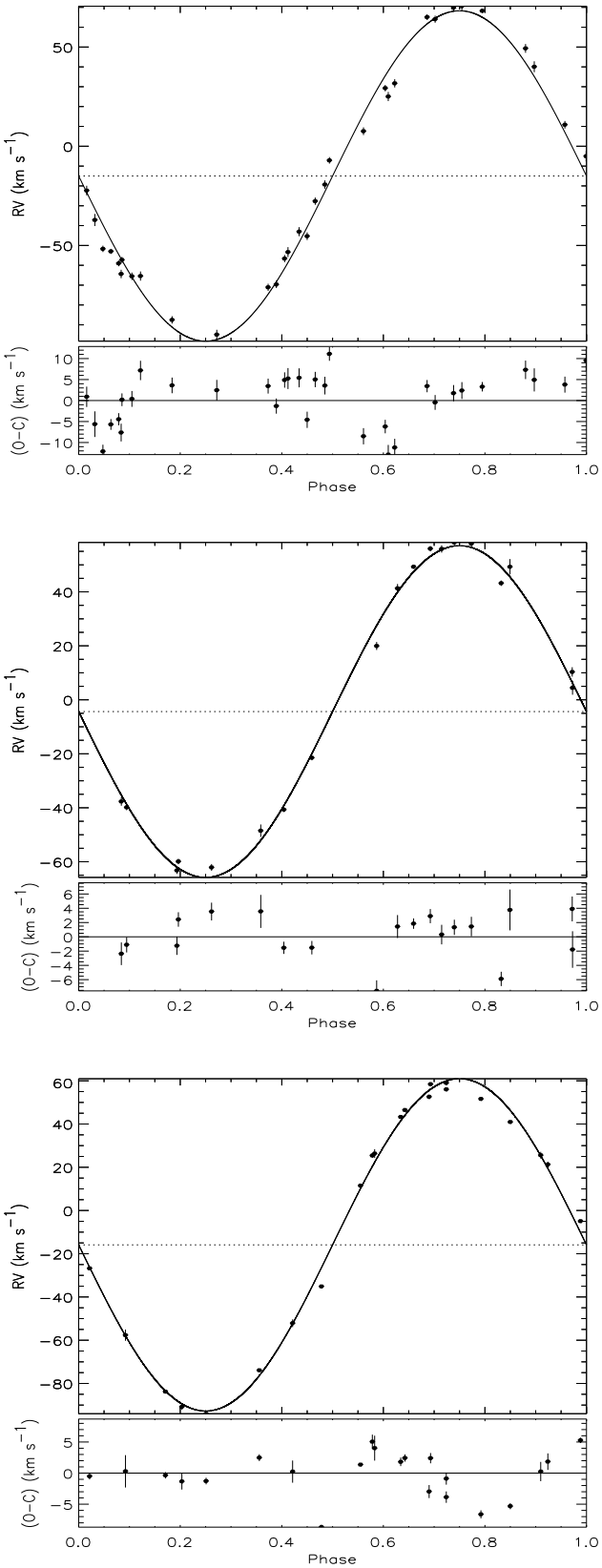


Figure 1. The theoretical v_r curves fit for the measured v_r values (upper panels) and the residuals (O-C) in km s^{-1} (lower panels). The left-hand, middle, and right-hand panels belong to GQ Dra, RR Lep, and TYC 683-640-1, respectively.

Input Catalog (TIC; Stassun et al. 2019) effective temperature ($T_{\rm eff}$)[3] values and projected rotational velocity ($v\sin i$) estimated from the fundamental parameters of the systems given in the literature studies (Erdem & Öztürk 2016; Ulaş et al. 2020, 2022). To generate the synthetic spectra, we used the line-blanketed, local-thermodynamic equilibrium ATLAS9 model atmospheres (Kurucz 1993) and the SYNTHE code (Kurucz & Avrett 1981) to obtain the theoretical spectra. The ATLAS9 models and SYNTHE program were used in further spectroscopic analysis as well.

In our first v_r measurements we found all targets as single-lined. However, to be sure about this feature, we also used some synthetic templates with lower $T_{\rm eff}$ values (4000, 5000, and 6000 K) that could be more suitable to detect the v_r shifts in the secondary, less luminous and cool components. However, no results were found to be different than the previous measurements. The measured v_r values of each system are given in Table A1.

The v_r measurements were then analysed using the `rvfit` program[4] that models the v_r data of double-lined, single-lined binaries, or exoplanets based on the minimization method of adaptive simulated annealing (Iglesias-Marzoa, López-Morales & Jesús Arévalo Morales 2015). The program fits the parameters of the orbital period $P_{\rm orb}$, the periastron passage time $T_{\rm p}$, the orbital eccentricity (e), the argument of the periastron (ω), v_r of the centre of mass (γ), projected semimajor axis ($a\sin i$, where i is orbital inclination) and the amplitude of v_r for the primary (p) and secondary (s) ($K_{p,\,s}$). The $P_{\rm orb}$ values of the systems were measured from the *TESS* data of the systems, and they were fixed during the v_r analysis. In the analysis, we first searched for e and ω parameters in addition to others. However, the first results showed that all systems have circular orbits. Hence, those parameters were fixed during further analysis. The results of the v_r analysis are given in Table 2. The theoretical v_r fits to the v_r measurements are shown in Fig. 1.

3.2 Determination of atmospheric parameters and chemical abundances

To perform accurate binary modelling, we should know the $T_{\rm eff}$ values. Therefore, before binary modelling, spectroscopic analysis was carried out to estimate the $T_{\rm eff}$, surface gravity ($\log g$), and chemical abundances of the primary components of the systems. As a result of v_r analysis, we found that all systems are single-lined. Thus, the effects of the secondary components in total flux should be negligible. Hence, we can treat the systems as single objects in the spectroscopic analysis. Just in that case, possible flux contributions could come from the secondary components; in the analysis, we used the spectra that were taken at around 0.45–0.55 orbital phase[5], where the secondary component is partially covered by the primary. If there is more than one spectrum taken around these orbital phases, those spectra were combined to obtain a higher SNR value and used in the spectral analysis.

Since the hydrogen (H) lines are the unique tools to estimate the $T_{\rm eff}$ value, we first utilized the H_β line for the determination of the $T_{\rm eff}$ parameters. The minimization method was used in the analysis as described by Catanzaro, Leone & Dall (2004). During the analysis of H_β line, we fixed the $\log g$ parameter and the metallicity as 4.0 and solar, respectively. Since there is no significant effect of $\log g$ on the de-

[3]GQ Dra: $T_{\rm eff} = 8936 \pm 371$ K, RR Lep: $T_{\rm eff} = 7928 \pm 163$ K, TYC 683-640-1: $T_{\rm eff} = 6802 \pm 130$ K

[4]http://www.cefca.es/people/riglesias/rvfit.html

[5]Preferable at 0.5 phase if it is available.

Downloaded from https://academic.oup.com/mnras/article/527/2/4076/7408619 by Canakkale Onsekiz Mart Universitesi user on 03 January 2024

Table 3. The Hβ $T_{\rm eff}$ values, the final atmospheric parameters, $v\sin i$ and the Fe abundances of the primary components of GQ Dra, RR Lep, and TYC 683-640-1. $\log\epsilon$ (Fe) is the relative abundance with respect to hydrogen (H = 12.0).

Star	Hβ line $T_{\rm eff}$ (K)	$T_{\rm eff}$ (K)	$\log g$ (cgs)	Fe lines ξ (km s^{-1})	$v\sin i$ (km s^{-1})	$\log\epsilon$ (Fe)
GQ Dra	8600 ± 200	8700 ± 100	4.0 ± 0.1	1.4 ± 0.2	130 ± 4	7.67 ± 0.16
RR Lep	7800 ± 150	7800 ± 100	4.1 ± 0.1	3.1 ± 0.2	119 ± 4	7.15 ± 0.17
TYC 683-640-1	7200 ± 150	7500 ± 100	3.9 ± 0.1	2.4 ± 0.3	63 ± 6	7.73 ± 0.60

termination of $T_{\rm eff}$ for the stars having $T_{\rm eff}$ lower than 8000 K for such systems, the $\log g$ does not affect the estimation of $T_{\rm eff}$ (Niemczura, Smalley & Pych 2014). Additionally, the metallicity does not affect the profile of hydrogen lines significantly; hence, the metallicity was fixed as solar during the determination of initial $T_{\rm eff}$ values of the systems. According to the analysis, we determined that GQ Dra, RR Lep, and TYC 683-640-1 have $T_{\rm eff}$ of 8600 ± 200, 7800 ± 150, and 7200 ± 150 K, respectively. Since the derived H_β $T_{\rm eff}$ values are around 8000 K for RR Lep and TYC 683-640-1, we did not search for $\log g$ parameters in the H_β line analysis for these systems. However, for GQ Dra, the $\log g$ value was searched for and found to be 3.9 ± 0.1. To estimate $\log g$, projected rotational velocity ($v\sin i$), and microturbulence (ξ) parameters for all systems, we carried out additional spectroscopic analysis based on the relationship between the ionization/excitation potential and chemical abundance of an element. Taking into account the H_β $T_{\rm eff}$ values of our systems, we preferred to use the iron (Fe) element in our analysis, as this element is found more abundant in such $T_{\rm eff}$ range. In this analysis, the spectrum synthesis method was used and the procedure described in the study of Kahraman Aliçavuş et al. (2016) was followed. The results of H_β and Fe lines' analyses are given in Table 3. The consistency between the theoretical models and observations is demonstrated in Fig. 2.

After the determination of the final atmospheric parameters, the chemical abundances of the individual elements could be derived. By taking into account the final atmospheric parameters as input and considering the spectrum synthesis method, the absorption lines of elements were modelled. In advance of the modelling, the line identification for each absorption line was carried out using the Kurucz line list.[6] As a result of this analysis, the chemical abundances of some elements were obtained for the primary component of the target systems. The derived chemical abundances for Fe and other elements are given in Tables 3 and A2, respectively. The chemical abundance distributions of the primary components of the target systems are shown in Fig. 3. When the chemical abundance distributions of the targets were investigated, the chemical abundances of the primary component of GQ Dra and RR Lep appeared to have abundances similar to the Sun (Asplund et al. 2009) within error bars. However, TYC 683-640-1 appeared to have overabundances in some elements such as Ca, Ti, Cr, and Ni. Even though the Fe abundance is similar to the Sun, the primary component of TYC 683-640-1 could be a slightly metal-rich star.

4 PHOTOMETRIC ANALYSIS

The *TESS* data of the targets were used in the photometric analysis. We utilized the resulting parameters of the spectroscopic analyses as input during the photometric investigation. Information about the TESS data is given in Section 2 and Table 1.

4.1 Binary modelling

To model the binary variation of the systems, first, the oscillation effects on the light curves were removed. This is because the oscillations could especially change the shape of the eclipses. For this reason, initially, we searched for the pulsation frequencies using the PERIOD04 program (Lenz & Breger 2005). The oscillation frequencies were then cleaned from the light curves. This procedure was applied for each *TESS* sector of the systems. After cleaning the oscillations, the light curves of the systems were phased using the parameters given in Table 2 and then normalized. Finally, these light curves of the systems were binned to 2000 points for the binary modelling.

The known binary modelling program of WILSON-DEVINNEY (W-D; Wilson & Devinney 1971) was used in the analysis and the uncertainties of the determined parameters were investigated with the Monte-Carlo simulations (Zola et al. 2004, 2010). In the binary modelling, we fixed some parameters such as $T_{\rm eff}$ of the primary component, the bolometric albedos (Ruciński 1969), the bolometric gravity-darkening coefficient (von Zeipel 1924), and the logarithmic limb darkening coefficient (van Hamme 1993) as the same given in the study of Kahraman Aliçavuş et al. (2022). Other parameters like mass ratio (q), dimensionless potential (Ω), $T_{\rm eff}$ of the secondary component, inclination (i), and phase shift (ϕ) were set free. During the analysis, we first decided on the binary configuration of the systems. Initially, the detached configuration and then the semidetached configuration were tested for each system. As a result, considering the goodness of fit parameter χ^2, we found that GQ Dra and RR Lep are semidetached systems, while TYC 683-640-1 is a detached binary. In the literature, GQ Dra (Ulaş et al. 2020) and TYC 683-640-1 (Ulaş et al. 2022) were also classified as semidetached and detached systems same as us, respectively. However, RR Lep is classified as a detached 'however near contact' system by Erdem & Öztürk (2016), but in this study, low-quality photometric data were used compared to *TESS* data. Hence, the difference in the configuration is caused by the photometric data quality.

After we decided on the binary configurations of the systems, a q-search was carried out. In the q search, all parameters were set free and the q value was fixed in each iteration from 0 to 1 with a step of 0.01. As a result of this examination, we obtained preliminary q values for each system considering the minimum χ^2. For GQ Dra, RR Lep, and TYC 683-640-1, the initial q parameters were found as 0.34 ± 0.02, 0.28 ± 0.02, and 0.50 ± 0.02, respectively. These q values were used as input for further binary modelling and were improved. Consequently, the best-fitting binary models for each system were determined. The consistency between the models and binary variations is shown in Fig. 4 and the results

[6] http://kurucz.harvard.edu/linelists.html

Downloaded from https://academic.oup.com/mnras/article/527/2/4076/7408619 by Canakkale Onsekiz Mart Universitesi user on 03 January 2024

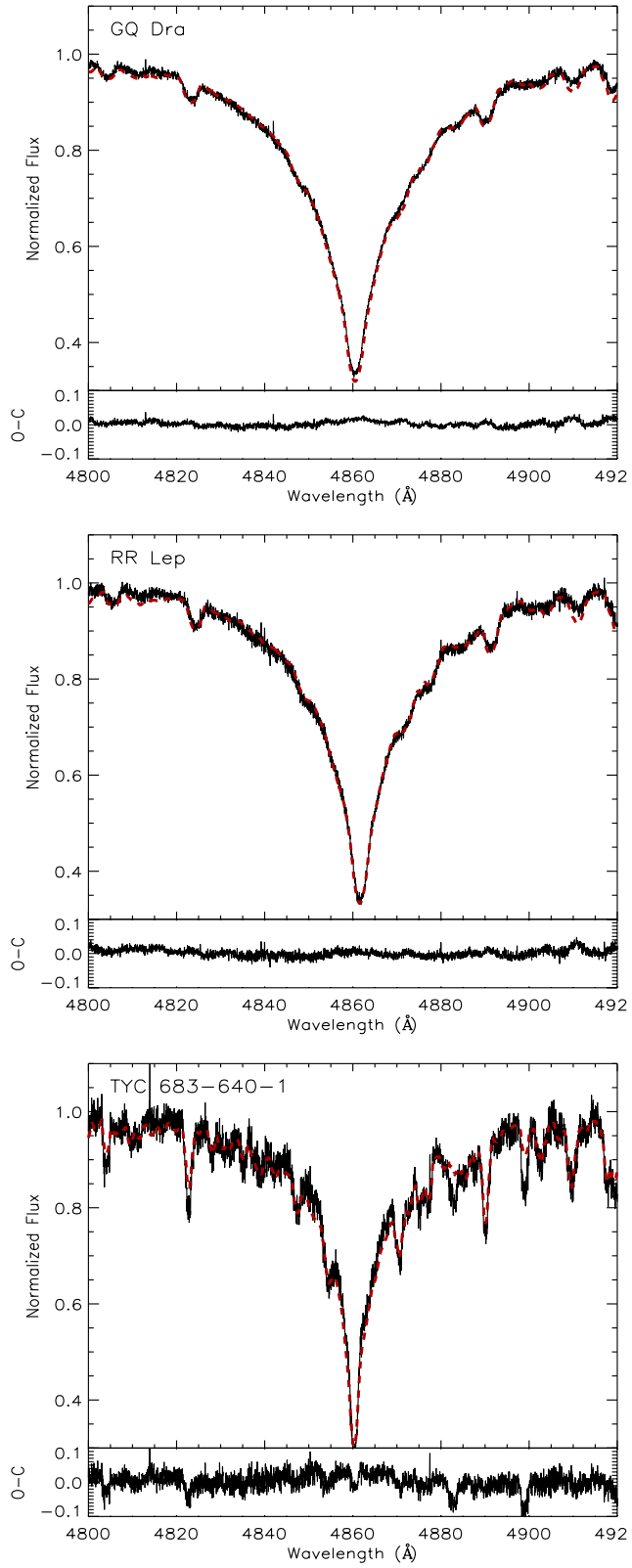


Figure 2. Top panels: The best theoretical fits to the observed H_β lines of GQ Dra, RR Lep, and TYC 683-640-1. Bottom panels: Residuals. For modelling, the H_β line metallicity of the models was taken as solar (Asplund et al. 2009). The significant residuals in TYC 683-640-1 are caused by the metallicity difference between the star and solar (see, Section 3.2).

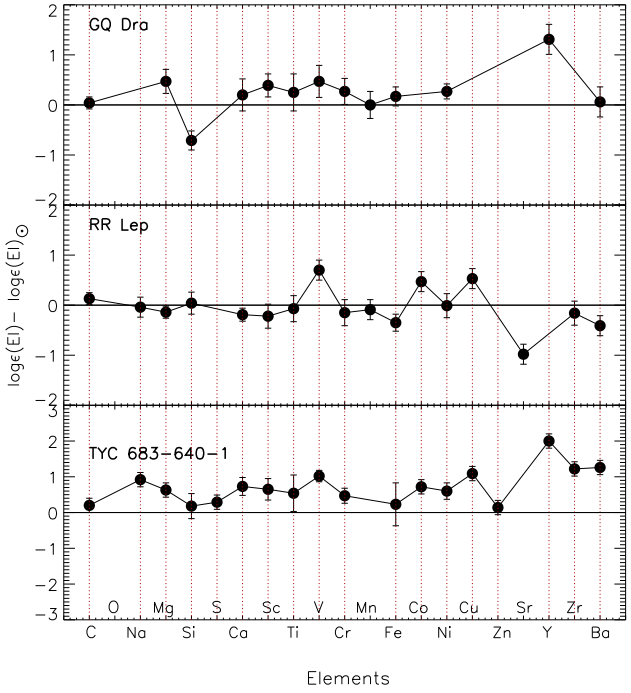


Figure 3. Chemical abundance distributions of the primary components of GQ Dra, RR Lep, and TYC 683-640-1 relative to solar chemical abundances (Asplund et al. 2009).

of the binary modelling are given in Table 4. Considering that the W-D errors are not very significant, the uncertainties of the given parameters were estimated with the help of Monte-Carlo simulations and additionally by changing the parameters such as albedo and gravity darkening with different values (e.g. Southworth 2020; Pavlovski et al. 2023). As a result, the uncertainties of the calculated parameters were obtained and they are given in Table 4.

The resulting parameters of the binary modellings were used to calculate the fundamental stellar parameters such as mass (M), radius (R), luminosity (L), bolometric (M_{bol}), and absolute (M_V) magnitudes. To compute these parameters, well-known Kepler, Pogson equations, and bolometric correction (BC) from the study of Eker et al. (2020) were used. These parameters are also given in Table 4.

4.2 Pulsation analysis

We carried out a pulsation analysis after removing the binary models from the light curves. The residuals were analysed using the PERIOD04 program (Lenz & Breger 2005). All TESS sector data of the systems were considered in the analysis. The significance limit for the frequencies was taken as 4.5 (Baran & Koen 2021). Taking into account the determined frequencies (see Tables 5 and 6) and the $T_{\rm eff}$ values of the systems, we could say that the pulsating stars are δ Scuti variables. Considering the $T_{\rm eff}$ values of the binary components of each system and also the $T_{\rm eff}$ range for the δ Scuti stars (6300–8600 K, Rodríguez & Breger, 2001), we concluded that in each system the more luminous, hotter, primary components are the pulsators. Only the secondary component of TYC 683-640-1 system could be a pulsator as well according to its $T_{\rm eff}$ value with the error bars. To be sure about the variability of this system

Downloaded from https://academic.oup.com/mnras/article/527/2/4076/7408619 by Canakkale Onsekiz Mart Universitesi user on 03 January 2024

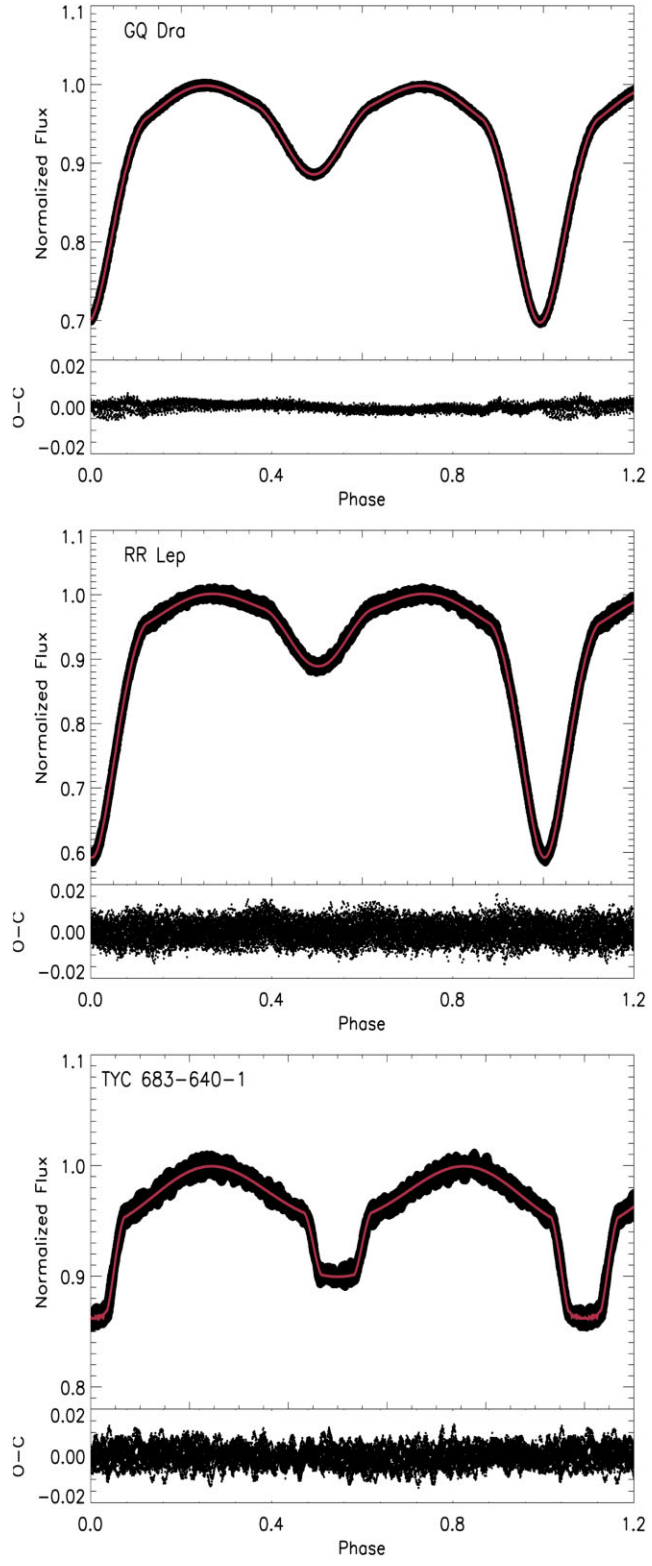


Figure 4. Top panels: The best binary modelling fits (red lines) to the *TESS* observation (black dots) of GQ Dra (left), RR Lep (middle), and TYC 683-640-1 (right). Bottom panels: Residuals.

using the calculated physical parameters and the pulsation constant equation ($Q = P\sqrt{\rho/\rho_{\odot}} = PM^{1/2}R^{-3/2}$), we computed expected frequencies for each binary component in TYC 683-640-1 taking into account the Q value 0.033 for the fundamental mode (Fitch 1981). As a result, the frequencies for primary and secondary binary components were found as 6.16 d^{-1} and 27.28 d^{-1}, respectively. In addition, according to the determined parameters given in Table 4, the luminosity (L) of the secondary component of TYC 683-640-1 is below the L value of the cool border of δ Scuti instability strip. Hence, the secondary system is not located inside the δ Scuti instability strip. Considering the determined frequencies for TYC 683-640-1 and the L value of the secondary component, we can say that the primary component is likely the oscillating star in the system.

Determined frequencies for each system were examined to control for possible modulations with the orbital period's frequency. As a result, we found that GQ Dra shows frequency modulations. In Fig. 5, the modulated frequencies by the frequency of the orbital period (1.305645 d^{-1}) are shown. Because of this modulation, the system was considered a possible tidally tilted pulsator. In the tidally tilted systems, frequencies of the pulsating stars are split by the orbital period's frequency, and its multiples. In addition, the pulsation amplitude is changed through the orbital phase (Handler et al. 2020; Rappaport et al. 2021). Therefore, we examined these properties to determine whether GQ Dra exhibits any of them using the procedure described in the study of Handler et al. (2020). In Fig. 6, in the top, middle, and bottom panels, respectively, the binary variation, pulsation amplitude variations, and the amplitude changes of the highest amplitude frequency with the orbital phase are shown. According to this figure, it is seen that at around 0.25 and 0.75 orbital phases, the pulsation amplitudes almost disappear compared to the other orbital phases. When the frequencies of GQ Dra were examined in detail, it was also found that independent frequencies are divided by the frequency of the orbital period or its multiples. The frequencies of GQ Dra are given in Table 5. Taking into account the results, we could conclude that GQ Dra is another candidate for tidally tilted pulsators.

RR Lep also shows frequency modulation with the orbital period and the frequency structure like GQ Dra (see, Table 5). However, this system does not have enough *TESS* data, hence the pulsation properties could not be examined in detail. The frequency modulation could also be caused by the orbital light time effect (Hey et al. 2020) but for such close binary systems with tight orbits, this effect will be too small to be detected. Therefore, RR Lep is considered to be a candidate tidally tilted pulsator. The frequency list for the pulsation component of RR Lep is given in Table 5. When the TYC 683-640-1 system was examined, we obtained that the system does not show similar behavior to other systems. It exhibits 12 independent frequencies given in Table 6. The amplitude spectra of the target systems are given in Fig. 7.

5 DISCUSSION AND CONCLUSIONS

The importance of eclipsing binary systems with pulsating components has been known for decades. In this study, three single-lined eclipsing binary systems with pulsating components, GQ Dra, RR Lep, and TYC 683-640-1, were analysed. We investigated these systems to reveal their pulsation structure and binary properties. First, a spectroscopic analysis was carried out to derive the orbital parameters from the radial velocity measurements and the atmospheric parameters for the more luminous primary compo-

Downloaded from https://academic.oup.com/mnras/article/527/2/4076/7408619 by Canakkale Onsekiz Mart Universitesi user on 03 January 2024

Table 4. Results of the binary modelling and the astrophysical parameters. The subscripts p, s, and 3 represent the primary, secondary, and third components. ^{a} and *l* show the fixed parameters and relative luminosity, respectively.

Parameter	GQ Dra	RR Lep	TYC 683-640-1
$i\,(^o)$	76.46 ± 0.31	79.12 ± 0.32	83.68 ± 0.30
$T_{effp}{}^a$ (K)	8700 ± 100	7800 ± 100	7500 ± 100
T_{effs} (K)	4997 ± 126	4232 ± 137	6215 ± 128
Ω_p	2.791 ± 0.010	2.833 ± 0.010	3.596 ± 0.020
Ω_s	2.536 ± 0.017	2.413 ± 0.016	6.435 ± 0.092
ϕ	-0.0073 ± 0.0001	0.0027 ± 0.0001	0.0001 ± 0.0002
q	0.348 ± 0.010	0.276 ± 0.010	0.503 ± 0.010
$r_p{}^*$ (mean)	0.416 ± 0.002	0.402 ± 0.002	0.329 ± 0.003
$r_s{}^*$ (mean)	0.290 ± 0.002	0.273 ± 0.002	0.097 ± 0.001
$l_p\,/\,(l_p + l_s)$	0.91 ± 0.02	0.95 ± 0.02	0.95 ± 0.02
$l_s\,/(l_p + l_s)$	0.09 ± 0.02	0.05 ± 0.02	0.05 ± 0.01
l_3	0.24 ± 0.03	0.03 ± 0.01	–
	Derived quantities		
M_p ($M_\odot$)	2.16 ± 0.16	1.79 ± 0.12	2.09 ± 0.10
M_s ($M_\odot$)	0.75 ± 0.02	0.50 ± 0.02	1.05 ± 0.02
R_p ($R_\odot$)	2.09 ± 0.05	2.10 ± 0.04	3.70 ± 0.08
R_s ($R_\odot$)	1.39 ± 0.04	1.35 ± 0.03	1.09 ± 0.07
$\log L_p$ ($L_\odot$)	1.35 ± 0.02	1.17 ± 0.02	1.59 ± 0.02
$\log L_s$ ($L_\odot$)	0.03 ± 0.01	-0.28 ± 0.02	0.20 ± 0.01
$\log g_p$ (cgs)	4.13 ± 0.04	4.05 ± 0.04	3.62 ± 0.04
$\log g_s$ (cgs)	4.03 ± 0.03	3.87 ± 0.03	4.39 ± 0.06
$M_{bolometricp}$ (mag)	1.37 ± 0.37	1.84 ± 0.35	0.78 ± 0.35
$M_{bolometrics}$ (mag)	4.67 ± 0.66	5.45 ± 0.81	4.25 ± 0.86
M_{Vp} (mag)	1.43 ± 0.39	1.80 ± 0.37	0.72 ± 0.37
M_{Vs} (mag)	4.93 ± 0.68	6.23 ± 0.83	4.20 ± 0.88

∗fractional radius, *R*/*a*.

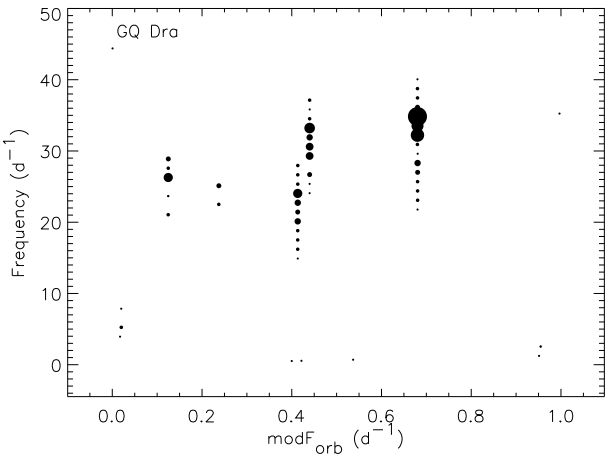


Figure 5. Modulation of the frequencies of GQ Dra with the frequency of the orbital period of $1.305645\,\mathrm{d}^{-1}$. The size of the symbols represents the amplitudes of pulsations.

nents. As a result, the orbital, atmospheric parameters, and in addition, the chemical abundances of the primary binary components were determined. Some of those quantities were used as input in the binary modelling. With the binary modelling, the fundamental stellar parameters (e.g. *M*, *R*) of the systems were derived.

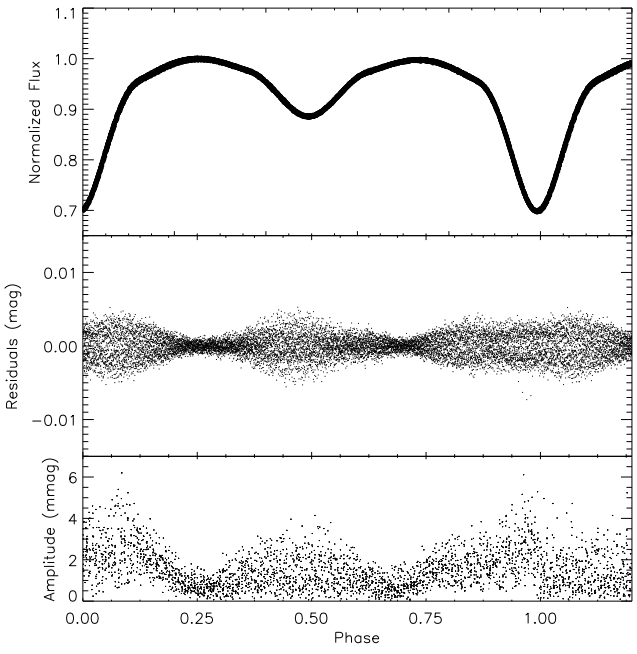


Figure 6. Top Panel: Phased light curve of GQ Dra. Middle panel: Pulsation amplitude variation of GQ Dra with the orbital phase. Bottom panel: Amplitude variation of highest amplitude independent pulsation frequency 34.8346^{-1} with the orbital phase.

Downloaded from https://academic.oup.com/mnras/article/527/2/4076/7408619 by Canakkale Onsekiz Mart Universitesi user on 03 January 2024

Table 5. The pulsation frequencies of GQ Dra and RR Lep. Error estimates for the independent frequencies and phases are given in parentheses.

	Frequency (d^{-1})	Amplitude (mmag)	Phase (radians)
	GQ Dra		
$\nu_1 - 10\nu_{orb}$	21.7784(1)	0.0663(5)	0.86(1)
$\nu_1 - 9\nu_{orb}$	23.0843(1)	0.1244(5)	0.49(1)
$\nu_1 - 8\nu_{orb}$	24.3895(1)	0.1324(5)	0.16(1)
$\nu_1 - 7\nu_{orb}$	25.6955(1)	0.0939(5)	0.47(2)
$\nu_1 - 6\nu_{orb}$	27.0013(1)	0.1957(5)	0.35(1)
$\nu_1 - 5\nu_{orb}$	28.3068(1)	0.4478(5)	0.54(1)
$\nu_1 - 3\nu_{orb}$	30.9176(1)	0.1578(5)	0.90(1)
$\nu_1 - 2\nu_{orb}$	32.2233(1)	1.5891(5)	0.04(1)
$\nu_1 - \nu_{orb}$	33.5291(1)	1.1255(5)	0.96(1)
ν_1	34.8346(1)	2.0376(5)	0.75(1)
$\nu_1 + \nu_{orb}$	36.1404(1)	0.1842(5)	0.23(1)
$\nu_1 + 2\nu_{orb}$	37.4460(1)	0.0985(5)	0.76(1)
$\nu_1 + 3\nu_{orb}$	38.7515(1)	0.1326(5)	0.58(1)
$\nu_1 + 4\nu_{orb}$	40.0572(1)	0.0723(5)	0.83(1)
$\nu_2 - 7\nu_{orb}$	24.0757(1)	0.0762(5)	0.27(1)
$\nu_2 - 6\nu_{orb}$	25.3817(1)	0.0702(5)	0.59(1)
$\nu_2 - 5\nu_{orb}$	26.6870(1)	0.1787(5)	0.88(1)
$\nu_2 - 3\nu_{orb}$	29.2983(1)	0.6048(5)	0.43(1)
$\nu_2 - 2\nu_{orb}$	30.6039(1)	0.6319(5)	0.25(1)
$\nu_2 - \nu_{orb}$	31.9096(1)	0.4155(5)	0.94(1)
ν_2	33.2152(1)	0.8354(5)	0.84(1)
$\nu_2 + \nu_{orb}$	34.5209(1)	0.0869(5)	0.51(1)
$\nu_2 + 2\nu_{orb}$	35.8266(1)	0.0820(5)	0.08(1)
$\nu_2 + 3\nu_{orb}$	37.1321(1)	0.1146(5)	0.33(1)
$\nu_3 - 7\nu_{orb}$	14.9017(1)	0.0824(5)	0.03(1)
$\nu_3 - 6\nu_{orb}$	16.2072(1)	0.0965(5)	0.68(1)
$\nu_3 - 5\nu_{orb}$	17.5129(1)	0.1496(5)	0.97(1)
$\nu_3 - 4\nu_{orb}$	18.8185(1)	0.1130(5)	0.26(1)
$\nu_3 - 3\nu_{orb}$	20.1241(1)	0.4828(5)	0.57(1)
$\nu_3 - 2\nu_{orb}$	21.4299(1)	0.2284(5)	0.34(1)
$\nu_3 - \nu_{orb}$	22.7356(1)	0.4038(5)	0.79(1)
ν_3	24.0411(1)	0.6691(5)	0.93(1)
$\nu_3 + \nu_{orb}$	25.3469(1)	0.01171(5)	0.39(1)
$\nu_3 + 2\nu_{orb}$	26.6525(1)	0.0862(5)	0.20(1)
$\nu_3 + 3\nu_{orb}$	27.9581(1)	0.1257(5)	0.04(1)
$\nu_4 - 4\nu_{orb}$	21.0529(1)	0.0981(5)	0.93(1)
$\nu_4 - 2\nu_{orb}$	23.6643(1)	0.0589(5)	0.64(1)
ν_4	26.2756(1)	0.6690(5)	0.22(1)
$\nu_4 + \nu_{orb}$	27.5812(1)	0.1543(5)	0.54(1)
$\nu_4 + 2\nu_{orb}$	28.8870(1)	0.2866(5)	0.49(1)
$\nu_5 - 2\nu_{orb}$	22.5057(1)	0.1172(5)	0.03(1)
ν_5	25.1172(1)	0.2204(5)	0.28(1)
ν_6	34.8468(1)	0.0825(5)	0.50(1)
$\nu_7 - \nu_{orb}$	32.2190(1)	0.0667(5)	0.96(1)
ν_7	33.5216(1)	0.0774(5)	0.45(1)
	RR Lep		
$\nu_1 - 2\nu_{orb}$	29.6795(1)	3.2503(2)	0.71(1)
$\nu_1 - \nu_{orb}$	30.7745(1)	0.6122(2)	0.67(1)
ν_1	31.8657(1)	3.4633(2)	0.65(1)
$\nu_2 - 2\nu_{orb}$	30.0915(3)	2.4292(2)	0.83(1)
$\nu_2 - \nu_{orb}$	33.3651(4)	0.9127(2)	0.51(1)
ν_2	32.2758(1)	2.4795(4)	0.18(1)
ν_3	25.7821(1)	1.2466(4)	0.48(1)
$\nu_3 + 2\nu_{orb}$	27.9645(4)	0.9400(2)	0.23(1)
$\nu_3 + 4\nu_{orb}$	30.1526(4)	1.2150(2)	0.77(1)
ν_4	23.6646(1)	1.2043	0.86(4)
$\nu_5 - 2\nu_{orb}$	24.2693(4)	0.7770(2)	0.96(1)
ν_6	32.4914(1)	0.9665(2)	0.05(1)
$\nu_6 + 2\nu_{orb}$	34.6776(1)	0.9534(2)	0.49(1)
ν_7	31.9858(1)	0.5322(2)	0.91(1)

Table 6. The pulsation frequencies of TYC 683-640-1. Error estimates for the independent frequencies and phases are given in parentheses.

	Frequency (d^{-1})	Amplitude (mmag)	Phase (radians)
ν_1	7.5638(1)	4.3445(2)	0.40(1)
ν_2	11.1392(1)	1.3032(2)	0.66(1)
ν_3	6.7684(1)	1.1798(2)	0.16(1)
ν_4	6.8568(1)	1.1310(2)	0.59(1)
ν_5	10.3861(1)	1.0657(2)	0.89(1)
ν_6	13.7636(1)	0.9923(2)	0.98(1)
ν_7	13.3121(1)	0.9841(2)	0.73(1)
ν_8	12.4956(1)	1.0962(2)	0.44(1)
ν_9	13.0431(1)	0.7788(2)	0.47(1)
ν_{10}	12.9451(1)	0.7283(2)	0.28(1)
ν_{11}	6.0268(1)	0.5776(2)	0.43(1)
ν_{12}	12.4494(1)	0.5754(2)	0.24(1)

We compared our results with the conclusions of the previous studies. For GQ Dra, Ulaş et al. (2020) carried out a binary modelling analysis. Their results show significant differences from ours. Especially, the difference in M and R parameters is significant. This discrepancy could be caused by the quality of the photometric data and the difference in the $T_{\rm eff}$ values. The RR Lep system was already studied by Liakos & Niarchos (2013). In this study, binary modelling was performed with ground-based photometric data. The results of this study and ours show a discrepancy in the parameters of the secondary component because of the noise level in the data. TYC 683-640-1 was investigated by Ulaş et al. (2022). For this system, there is also a significant difference between the M and R values. All differences in this and other systems are probably caused by the pulsations in addition to the data quality. Especially, TYC 683-640-1 exhibits high amplitude pulsations that affect the shapes of eclipses. If the pulsations are not removed before the binary modelling, they would affect the sensitivity of the resulting parameters because of the high-amplitude oscillation. Hence, the source of this difference in TYC 683-640-1 is probably the pulsation effects.

The pulsational behaviour of the target systems was examined and the primary components of the systems were classified as δ Scuti variables. Their positions were shown in the Hertzsprung–Russell (H-R) diagram in Fig. 8. All the primary components were found to be located inside the δ Scuti instability strip. In addition, we found that two systems, GQ Dra and RR Lep, are strong candidates of tidally tilted pulsators. Tidally tilted pulsators are a new type of oscillating object. Their frequencies are modulated with the orbital period and they show oscillations that are dominant in one part of the pulsating star. The number of known tidally tilted objects is less than 10 [e.g. CO Cam (Kurtz et al.,2020), TIC 63328020 (Rappaport et al.,2021), HD 265435 (Jayaraman et al., 2022), TZ Dra (Kahraman Aliçavuş et al., 2022)], and all properties of such systems are not known yet. Hence, the increasing number of such systems is important to investigate them in detail. With this study, we determined the fundamental stellar parameters of three important eclipsing binaries with δ Scuti pulsators. Such systems are unique since they give us sensitive stellar parameters needed for accurate theoretical modelling.

Downloaded from https://academic.oup.com/mnras/article/527/2/4076/7408619 by Canakkale Onsekiz Mart Universitesi user on 03 January 2024

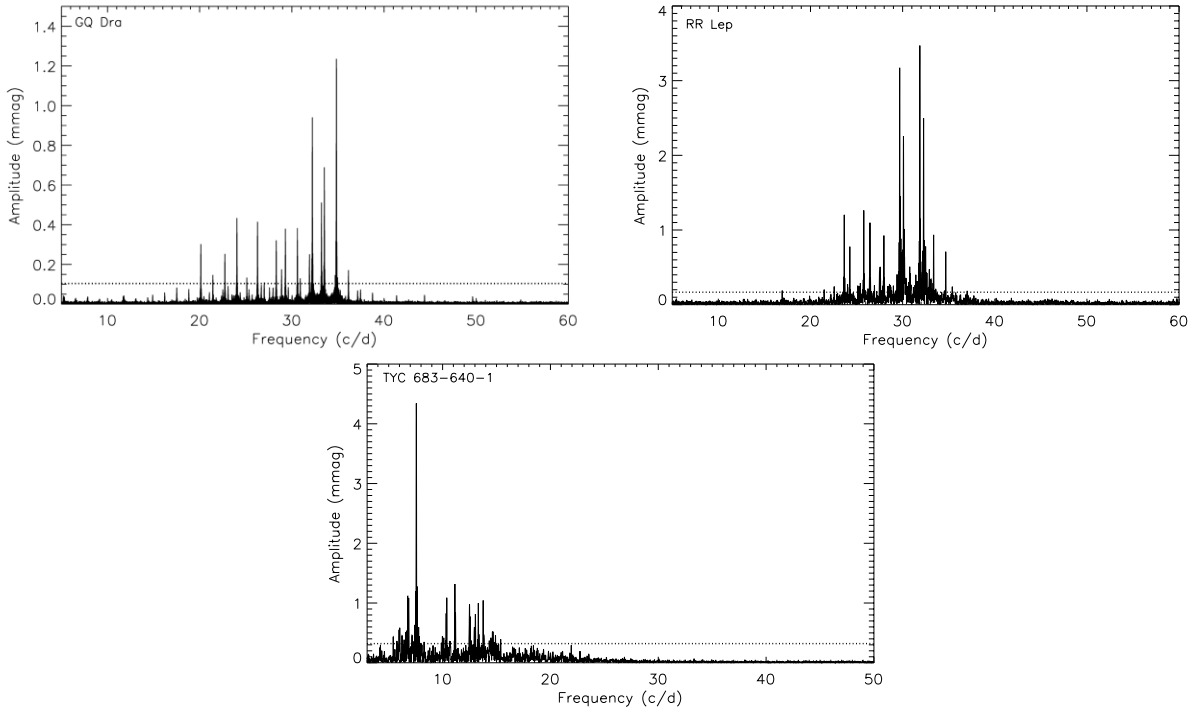


Figure 7. The amplitude spectra of the targets. The dashed lines represent the 4.5σ level.

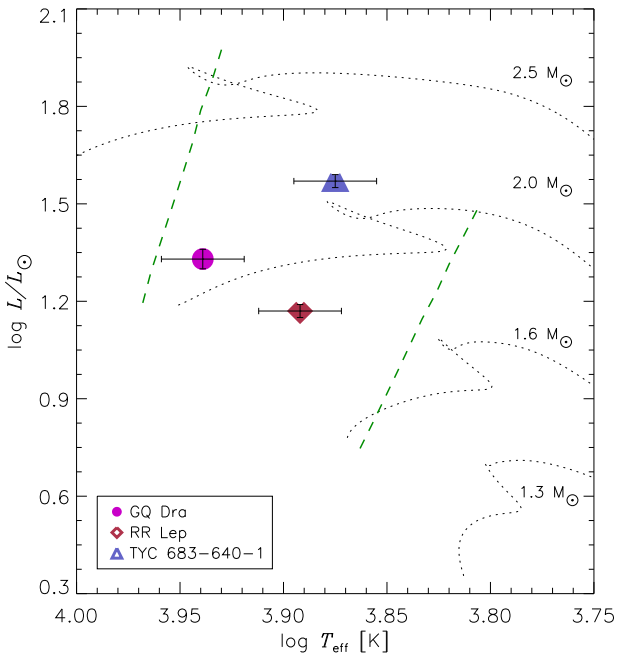


Figure 8. The positions of the primary binary components in the H-R diagram. The instability strip borders of the δ Scuti stars, and evolution tracks were taken from Murphy et al. (2019) and Kahraman Aliçavuş et al. (2016), respectively.

ACKNOWLEDGEMENTS

The authors would like to thank the reviewer for useful comments and suggestions that helped to improve the publication. This study has been supported by the Scientific and Technological Research Council (TUBITAK) project through 120F330. GH thanks the Polish National Center for Science (NCN) for supporting the study through grants 2015/18/A/ST9/00578 and 2021/43/B/ST9/02972. Based on observations made with the Mercator Telescope, operated on the island of La Palma by the Flemish Community, at the Spanish Observatorio del Roque de los Muchachos of the Instituto de Astrofìsica de Canarias. The TESS data presented in this paper were obtained from the Mikulski Archive for Space Telescopes (MAST). Funding for the TESS mission is provided by the NASA Explorer Program. This work has made use of data from the European Space Agency (ESA) mission Gaia (http://www.cosmos.esa.int/gaia), processed by the Gaia Data Processing and Analysis Consortium (DPAC, http://www.cosmos.esa.int/web/gaia/dpac/consortium). Funding for the DPAC has been provided by national institutions, in particular, the institutions participating in the Gaia Multilateral Agreement. This research has made use of the SIMBAD data base, operated at CDS, Strasbourq, France.

DATA AVAILABILITY

The data underlying this work will be shared at reasonable request to the corresponding author.

REFERENCES

Aerts C., Christensen-Dalsgaard J., Kurtz D. W., 2010, Asteroseismology, Astronomy and Astrophysics Library, Springer Science+Business Media B.V.
Asplund M., Grevesse N., Sauval A. J., Scott P., 2009, ARA&A, 47, 481
Baran A. S., Koen C., 2021, Acta Astron., 71, 113
Catanzaro G., Leone F., Dall T. H., 2004, A&A, 425, 641
Chang S.-W., Protopapas P., Kim D.-W., Byun Y.-I., 2013, AJ, 145, 132
Eker Z. et al., 2020, MNRAS, 496, 3887
Erdem A., Öztürk O., 2016, NewA, 48, 33
ESA, 1997, ESA Special Publication, 1200
Fitch W. S., 1981, ApJ, 249, 218

Downloaded from https://academic.oup.com/mnras/article/527/2/4076/7408619 by Canakkale Onsekiz Mart Universitesi user on 03 January 2024

Handler G. et al., 2020, Nature Astron., 4, 684
Hey D. R., Murphy S. J., Foreman-Mackey D., Bedding T. R., Pope B. J. S., Hogg D. W., 2020, AJ, 159, 202
Høg E. et al., 2000, A&A, 355, L27
Hoffmeister C., 1931, AN, 242, 129
Iglesias-Marzoa R., López-Morales M., Jesús Arévalo Morales M., 2015, PASP, 127, 567
Jayaraman R., Handler G., Rappaport S. A., Fuller J., Kurtz D. W., Charpinet S., Ricker G. R., 2022, ApJL, 928, L14
Kahraman Aliçavuş F. et al., 2016, MNRAS, 458, 2307
Kahraman Aliçavuş F., Soydugan E., Smalley B., Kubát J., 2017, MNRAS, 470, 915
Kahraman Aliçavuş F., Gümüş D., Kırmızıtaş Ö., Ekinci Ö., Çavuş S., Kaya Y. T., Aliçavuş F., 2022, Res. Astron. Astrophys., 22, 085003
Kahraman Aliçavuş F. et al., 2022, MNRAS, 510, 1413
Kahraman Aliçavuş F., Çoban Ç. G., Çelik E., Dogan D. S., Ekinci O., Aliçavuş F., 2023, MNRAS, 524, 619
Kreiner J. M., 2004, Acta Astron., 54, 207
Kurtz D. W. et al., 2020, MNRAS, 494, 5118
Kurucz R. L., Avrett E. H., 1981, SAO Special Rep., 391, 391
Kurucz R., 1993, Kurucz CD-ROM, Smithsonian Astrophysical Observatory, Cambridge
Lampens P., 2021, Galax, 9, 28
Lenz P., Breger M., 2005, Commun. Asterioseismol., 146, 53
Liakos A., Niarchos P., 2013, Ap&SS, 343, 123
Liakos A., Niarchos P., 2017, MNRAS, 465, 1181
Murphy S., Hey D., Van Reeth T., Bedding T., 2019, MNRAS, 485, 2380
Niemczura E., Smalley B., Pych W., 2014, in EwaNiemczura, BarrySmalley, WojtekPych, eds., Determination of Atmospheric Parameters of B-, A-, F- and G-Type Stars. Series: GeoPlanet: Earth and Planetary Sciences, Springer International Publishing
Pavlovski K., Southworth J., Tkachenko A., Van Reeth T., Tamajo E., 2023, A&A, 671, A139
Rappaport S. A. et al., 2021, MNRAS, 503, 254
Raskin G. et al., 2011, A&A, 526, A69
Ricker G. R. et al., 2014, SPIE, 9143, 914320
Rodríguez E., Breger M., 2001, A&A, 366, 178
Ruciński S. M., 1969, Acta Astron., 19, 245
Southworth J., 2020, Observatory, 140, 247
Stassun K. G. et al., 2019, AJ, 158, 138
Tody D., 1986, SPIE, 627, 733
Ulaş B. et al., 2020, Acta Astron., 70, 219
Ulaş B., Ulusoy C., Erkan N., Madiba M., Matsete M., 2022, Ap&SS, 367, 22
Wilson R. E., Devinney E. J., 1971, ApJ, 166, 605
van Hamme W., 1993, AJ, 106, 2096
von Zeipel H., 1924, MNRAS, 84, 665
Zola S. et al., 2004, Acta Astron., 54, 299
Zola S., Gazeas K., Kreiner J. M., Ogloza W., Siwak M., Koziel-Wierzbowska D., Winiarski M., 2010, MNRAS, 408, 464

APPENDIX

Table A1. Radial velocity measurements.

GQ Dra		RR Lep		TYC 683-640-1	
JD 2458000 +	v_r (km s^{-1})	JD 2458000 +	v_r (km s^{-1})	JD 2458000 +	v_r (km s^{-1})
986.5932	− 64.37 ± 2.12	1148.6426	49.29 ± 0.73	1161.5732	− 52.12 ± 1.76
988.5279	25.05 ± 2.306	1148.6727	56.00 ± 0.99	1161.7130	− 35.71 ± 0.40
1052.4623	− 57.29 ± 1.52	1161.6189	43.20 ± 1.01	1162.4861	51.62 ± 0.65
1052.4773	− 65.55 ± 1.89	1161.7470	10.32 ± 1.74	1162.6284	40.95 ± 0.49
1052.4902	− 65.43 ± 2.31	1162.7652	− 37.66 ± 1.59	1233.4901	43.28 ± 0.69
1053.4486	− 71.09 ± 1.78	1194.5267	57.86 ± 1.36	1233.5104	46.48 ± 0.59
1053.4610	− 69.67 ± 1.81	1230.5302	− 54.96 ± 1.75	1234.4436	− 26.76 ± 0.52
1053.4735	− 56.62 ± 1.83	1231.4448	− 39.83 ± 1.07	1237.4702	− 93.99 ± 0.53
1053.4786	− 53.35 ± 1.50	1234.4751	− 40.70 ± 0.86	1253.4055	56.03 ± 0.92
1054.4543	65.07 ± 1.46	1235.5580	19.95 ± 1.49	1253.4055	59.01 ± 0.99
1054.4664	64.02 ± 1.77	1236.5112	41.31 ± 1.61	1254.5059	− 83.77 ± 0.51
1054.4942	69.79 ± 1.94	1237.5292	58.29 ± 1.06	1255.4516	11.51 ± 0.40
1054.5375	68.25 ± 1.12	1253.5125	− 59.90 ± 1.01	1256.5179	− 4.93 ± 0.43
1055.4600	− 5.02 ± 2.64	1254.4879	− 62.09 ± 1.25	1257.4226	− 73.90 ± 0.55
1055.4727	− 22.34 ± 2.42	1256.4999	− 21.47 ± 0.94	1879.6145	− 57.67 ± 1.60
1055.4850	− 37.16 ± 3.06	1880.6959	− 63.20 ± 1.28	1910.6352	58.42 ± 0.83
1055.4972	− 51.72 ± 1.59	1960.5042	− 48.50 ± 1.76	1913.6657	21.26 ± 1.33
1055.5092	− 52.99 ± 1.28	2008.4416	55.89 ± 1.89	1957.4028	52.90 ± 1.41
1055.5210	− 59.028 ± 1.46	2010.3959	49.28 ± 1.41	1959.6006	26.33 ± 1.71
1056.4348	− 94.95 ± 2.46	2011.4243	4.44 ± 2.56	1960.4056	25.57 ± 1.55
1057.4220	7.59 ± 1.94			2006.3639	25.44 ± 1.13
1058.4323	49.32 ± 2.21				
1059.4310	− 87.52 ± 1.86				
1060.4274	− 19.31 ± 2.11				
1089.4929	− 43.04 ± 2.26				
1089.5050	− 45.33 ± 1.94				
1089.5172	− 27.69 ± 1.83				
1089.5386	− 7.12 ± 1.64				
1090.5043	70.59 ± 2.01				
1093.4523	29.29 ± 1.61				
1093.4666	31.70 ± 2.08				
1114.3565	40.05 ± 2.75				
1114.4027	10.82 ± 1.91				

Downloaded from https://academic.oup.com/mnras/article/527/2/4076/7408619 by Canakkale Onsekiz Mart Universitesi user on 03 January 2024

Table A2. Abundances of individual elements of the component stars. The number of the analysed spectral parts is given in parentheses.

Elements	GQ Dra	RR Lep	TYC 683-640-1
$_{6}$C	8.47 ± 0.35 (2)	8.56 ± 0.22 (5)	8.63 ± 0.20 (2)
$_{11}$Na		6.20 ± 0.20 (1)	7.16 ± 0.20 (2)
$_{12}$Mg	8.07 ± 0.34 (5)	7.46 ± 0.22 (3)	8.23 ± 0.37 (2)
$_{14}$Si	6.80 ± 0.29 (3)	7.55 ± 0.32 (5)	7.69 ± 0.35 (7)
$_{20}$Ca	6.54 ± 0.42 (4)	6.15 ± 0.23 (4)	7.07 ± 0.35 (11)
$_{21}$Sc	3.54 ± 0.20 (2)	2.93 ± 0.34 (3)	3.80 ± 0.30 (4)
$_{22}$Ti	5.20 ± 0.46 (12)	4.88 ± 0.36 (11)	5.49 ± 0.51 (25)
$_{23}$V		4.63 ± 0.20 (2)	4.95 ± 0.26 (4)
$_{24}$Cr	5.91 ± 0.27 (6)	5.49 ± 0.36 (9)	6.11 ± 0.31 (14)
$_{25}$Mn	5.43 ± 0.20 (1)	5.34 ± 0.20 (2)	
$_{26}$Fe	7.67 ± 0.26 (28)	7.15 ± 0.27 (29)	7.73 ± 0.60 (71)
$_{27}$Co		5.46 ± 0.20 (2)	5.71 ± 0.20 (1)
$_{28}$Ni	6.49 ± 0.26 (5)	6.21 ± 0.34 (7)	6.82 ± 0.23 (16)
$_{29}$Cu		4.72 ± 0.20 (1)	5.28 ± 0.20 (1)
$_{30}$Zn			4.70 ± 0.20 (1)
$_{38}$Sr	3.06 ± 0.20 (1)	1.89 ± 0.20 (1)	
$_{39}$Y	3.52 ± 0.20 (1)		4.21 ± 0.20 (2)
$_{40}$Zr		2.42 ± 0.34 (3)	3.80 ± 0.20 (2)
$_{56}$Ba	2.24 ± 0.20 (2)	1.77 ± 0.20 (2)	3.44 ± 0.20 (1)

This paper has been typeset from a TEX/LATEX file prepared by the author.

Downloaded from https://academic.oup.com/mnras/article/527/2/4076/7408619 by Canakkale Onsekiz Mart Universitesi user on 03 January 2024

© 2023 The Author(s)
Published by Oxford University Press on behalf of Royal Astronomical Society. This is an Open Access article distributed under the terms of the Creative Commons Attribution License (https://creativecommons.org/licenses/by/4.0/), which permits unrestricted reuse, distribution, and reproduction in any medium, provided the original work is properly cited.